Electric field gradients in ^{111}In-doped $(Hf/Zr)_3Al_2$ and $(Hf/Zr)_4Al_3$ mixed compounds: *ab initio* calculations, perturbed angular correlation measurements and site preference

2010 J. Phys.: Condens. Matter 22 215501

(http://iopscience.iop.org/0953-8984/22/21/215501)

J. Phys.: Condens. Matter **22** (2010) 215501 (10pp) doi:10.1088/0953-8984/22/21/215501

Electric field gradients in ^{111}In-doped $(Hf/Zr)_3Al_2$ and $(Hf/Zr)_4Al_3$ mixed compounds: *ab initio* calculations, perturbed angular correlation measurements and site preference

L A Errico[1,2], H M Petrilli[3], L A Terrazos[4], A Kulińska[5,6], P Wodniecki[5], K P Lieb[6], M Uhrmacher[6], J Belosevic-Cavor[7] and V Koteski[7]

[1] Departamento de Física and Instituto de Física La Plata (IFLP, CONICET-UNLP), Facultad de Ciencias Exactas, Universidad Nacional de La Plata, CC 67, 1900 La Plata, Argentina
[2] Universidad Nacional del Noroeste Bonaerense (UNNOBA), Monteagudo 2772, Pergamino, CP 2700, Buenos Aires, Argentina
[3] Instituto de Fisica, Universidade de Sao Paulo, CP 66318, 05315-970 Sao Paulo, SP, Brazil
[4] Universidade Federal de Campina Grande, Centro de Educação e Saude, Cuite PB 5817-000, Brazil
[5] Institute of Nuclear Physics Polish Academy of Sciences, Radzikowskiego 152, 31-342 Kraków, Poland
[6] II. Physikalisches Institut, Georg-August-Universität Göttingen, Friedrich-Hund-Platz 1, D-37077 Göttingen, Germany
[7] VINCA Institute of Nuclear Sciences, 11001 Belgrade, Serbia

Received 23 December 2009, in final form 15 March 2010
Published 30 April 2010
Online at stacks.iop.org/JPhysCM/22/215501

Abstract
The quadrupolar hyperfine interactions of in-diffused $^{111}In \rightarrow {}^{111}Cd$ probes in polycrystalline isostructural Zr_4Al_3 and Hf_4Al_3 samples containing small admixtures of the phases $(Zr/Hf)_3Al_2$ were investigated. A strong preference of ^{111}In solutes for the contaminant $(Zr/Hf)_3Al_2$ minority phases was observed. Detailed calculations of the electric field gradient (EFG) at the Cd nucleus using the full-potential augmented plane wave + local orbital formalism allowed us to assign the observed EFG fractions to the various lattice sites in the $(Zr/Hf)_3Al_2$ compounds and to understand the preferential site occupation of the minority phases by the ^{111}In atoms. The effects of the size of the supercell and relaxation around the oversized In and Cd probe atoms were investigated in detail.

1. Introduction

Hyperfine interaction techniques such as perturbed angular correlation (PAC) and Mössbauer spectroscopy can provide structural analysis of intermetallic compounds doped with very low concentrations of impurity (probe) atoms and often lead to definite conclusions on their lattice locations in polycrystalline materials [1–3]. In the last decade, a systematic study of the electric field gradients (EFG) of $^{181}Hf/^{181}Ta$ and $^{111}In/^{111}Cd$ probe nuclei in the full series of hafnium and zirconium aluminides has been carried out, intermetallic compounds which exhibit a large range of rather simple lattice structures [3–11]. Recently, successful attempts have been made for the compounds Zr_4Al_3 and Hf_4Al_3 to assign the hyperfine interaction parameters of $^{181}Hf/^{181}Ta$ probes to the possible Hf and Zr lattice sites [2] and even to distinguish among the lattice structures deduced from x-ray diffraction [12]. The $(Hf/Zr)_4Al_3$ phase structure can be

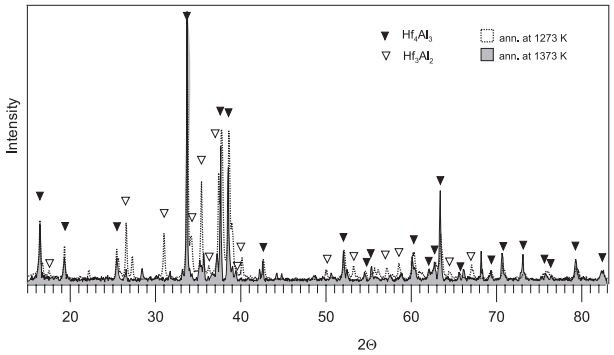

Figure 1. X-ray diffraction spectra of a mixed Hf_4Al_3–Hf_3Al_2 sample after annealing at 1273 and 1373 K. The expected diffraction peaks of Hf_4Al_3 and Hf_3Al_2 according to the JCPDS database are marked.

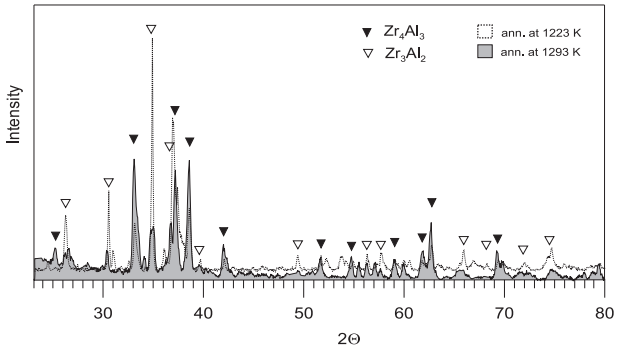

Figure 2. Same as figure 1 for a mixed Zr_4Al_3–Zr_3Al_2 sample after annealing at 1223 and 1293 K and compared with the JCPDS database standards of Zr_4Al_3 and Zr_3Al_2.

described as $P6/mmm$ (No 191) with one 3f (mmm) Wyckoff position of low symmetry for the Al atoms and two axially symmetric positions, labeled 2d ($-6m2$) and 2e ($6mm$), for the Zr/Hf atoms [4, 11]. Indeed, the two EFGs measured by means of PAC spectroscopy with ^{181}Hf/^{181}Ta probes have given evidence of substitutional Zr/Hf sites [2], as confirmed by EFG calculations using the full-potential augmented plane wave + local orbital formalism [13, 14]. As expected, in all the investigated hafnium and zirconium aluminides [4–9], the ^{181}Hf/^{181}Ta probes were found to occupy all the possible, non-equivalent Hf/Zr crystallographic sites.

The present work addresses the much more complicated problem of which lattice sites ^{111}In/^{111}Cd probes prefer in these aluminides. Evidently these probe atoms are different from the constituents of the compounds. Frequently, probe positions are tentatively attributed on the basis of either the EFG asymmetry parameter predicted by the point charge model, or by arguments of the atomic volumes and charges of solute and host atoms. However, such simplistic predictions often fail, as has been demonstrated for several Hf–Al and Zr–Al compounds. In the case of dilute $^{111}\text{In} \rightarrow {}^{111}$Cd impurities in these aluminides it has been observed that some of the Zr/Hf sites may be preferred [9]. Indium and aluminum, belonging to the same group in the periodic table, and with their small difference in electronegativity clearly would favor substitution of Al atoms by the In probes. On the other hand, the atomic radii [15] favor oversized In impurities to substitute Hf or Zr instead of Al. This 'competition' between atomic size and electronegativity occurs in various Hf and Zr aluminides and, indeed in the case of ^{111}In-doped $HfAl_2$ [6], a reversible switching process between both types of lattice sites with temperature occurs.

A different type of site preference has been observed in a mixture of ZrAl and Zr_2Al_3 phases, where ^{111}In segregates in the trace Zr_2Al_3 phase [7]. Similar segregations of In solutes in two-phase mixtures have been found by Collins and Zacate [1] in the case of the Pd–Ga, Ni–Al and Fe–Al systems. Preference of a solute for a certain phase occurs when the difference in the Gibbs free energy ΔG is different from zero and is termed segregation to the phase with lower energy. Even small differences in enthalpy may produce a high degree of segregation.

In view of these uncertainties, we report here on the measurement and interpretation of the quadrupole interactions of $^{111}\text{In} \rightarrow {}^{111}$Cd impurities dissolved in $(Zr/Hf)_4Al_3$, in the presence of small $(Zr/Hf)_3Al_2$ phase admixtures. Preliminary results for the measured EFGs of ^{111}Cd in these mixed $(Zr/Hf)_4Al_3$ samples have been reported in [11]. Experimental results on the hyperfine interaction of implanted $^{111}\text{In} \rightarrow {}^{111}$Cd ions in $(Zr/Hf)_3Al_2$ have been communicated in [9]. Considering the occurrence of phase mixtures and a large number of possible lattice sites in each phase, it is only through first-principles EFG calculations of dilute ^{111}Cd atoms that unambiguous evidence for the lattice sites selected by the ^{111}In probes in these aluminides can be achieved. This has been recently demonstrated for the case of dilute Cd impurities in the Laves phase $(Hf/Zr)Al_2$ [10]. In the course of the present calculations, several effects have been considered influencing the EFGs, such as lattice distortions due to the oversized Cd probe atoms, the size of the supercell embedding the probes and the type of first-principles approximations.

2. Experimental details

Samples of Zr_4Al_3 (42.8 at.% Al) and Hf_4Al_3 (43.2 at.% Al) were produced by arc melting, under an argon atmosphere. During melting of the samples, they were doped with the carrier-free ^{111}In activity and annealed in evacuated and sealed quartz tubes at different temperatures. The nominal sample compositions were determined by the masses of the components. Small mass losses during arc melting were assumed to be caused by evaporation of the more volatile Al element. The Hf–Al and Zr–Al phase diagrams around 42.85 at.% Al concentration corresponding to $(Hf/Zr)_4Al_3$ stoichiometry are rather complicated [4], in particular for the Zr–Al system, and we did not succeed in synthesizing single-phase samples. Phase analyses done by means of x-ray powder diffraction (XRD) established the structure of the investigated samples being predominantly $(Hf/Zr)_4Al_3$ with some admixtures of the $(Hf/Zr)_3Al_2$ phases, whose intensities strongly decreased for increasing annealing temperature. The respective x-ray diffraction spectra are illustrated in figures 1 and 2 for annealing temperatures ranging up to 1373 K. Annealing of the Hf_4Al_3 sample was done at 1223 K (1 day)

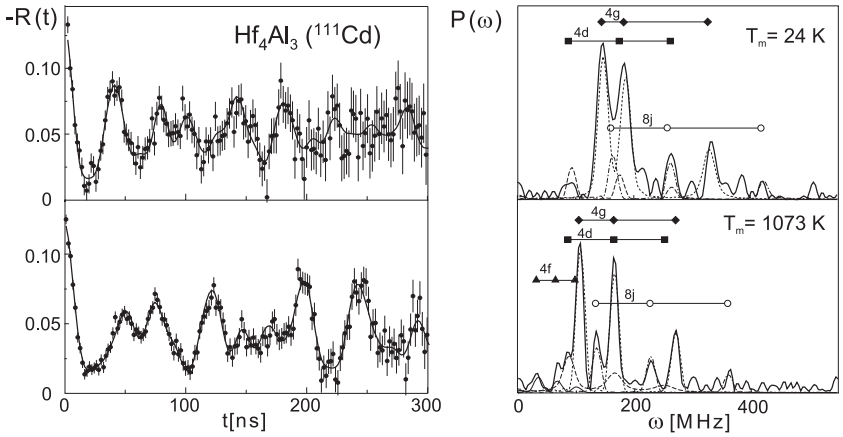

Figure 3. PAC spectra $-R(t)$ and their Fourier transforms $P(\omega)$ measured at 24 and 1073 K for ^{111}Cd in the Hf_4Al_3 sample annealed at 1373 K.

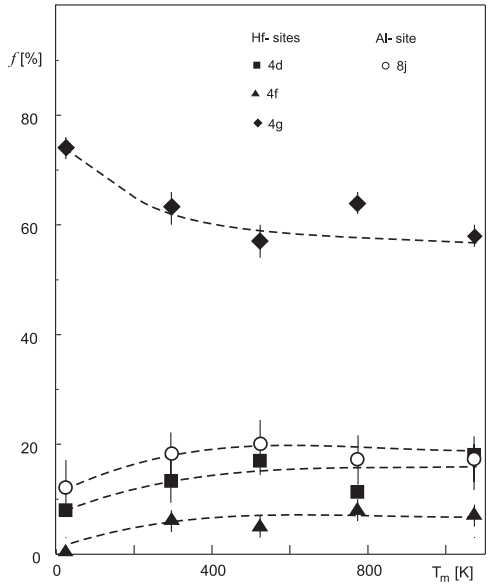

Figure 4. Temperature behavior of the various ^{111}Cd probe fractions in the Hf_4Al_3 sample. The 4(d), 4(f), 4(g) and 8(j) crystallographic sites relate to the Hf_3Al_2 minority phase.

and then at 1373 K (1 day), annealing of the Zr_4Al_3 sample at 1223 K (1 day) and afterwards at 1293 K (3 days).

The PAC experiments were carried out in the temperature range between 24 and 1100 K, those above 300 K using a small resistive oven of a low γ-ray absorption, and those below room temperature in a closed-cycle helium cryostat. A four BaF_2 detector apparatus which had a time resolution of 0.8 ns for the 171–245 keV cascade in ^{111}Cd was used.

For polycrystalline samples and a nuclear spin $I = 5/2$ of the intermediate nuclear level of the cascade, the perturbation factor $G_{22}(t)$ for static electric quadrupole interactions has the form [16]

$$G_{22}(t) = \sum_{i=1}^{k} f_i \sum_{n=0}^{3} s_{2n}(\eta_i) \cos(g_n(\eta_i)\nu_{Qi}t) \exp(-g_n(\eta_i)\delta_i t) \quad (1)$$

where f_i is the relative fraction of nuclei that experience a given perturbation. No texture was present in the samples. The various observed fractions f_i with different PAC parameters indicate the population of non-equivalent probe sites in the sample. The frequencies ω_n are related to the quadrupole frequency $\nu_Q = eQV_{33}/h$ by $\omega_n = g_n(\eta)\nu_Q$. The g_n and s_{2n} coefficients are known functions [17] of the asymmetry parameter $\eta = (V_{XX} - V_{YY})/V_{ZZ}$, where V_{ii} are the components of the diagonalized EFG tensor arbitrarily chosen as $|V_{XX}| \leqslant |V_{YY}| \leqslant |V_{ZZ}|$. The exponential functions account for a Lorentzian frequency distribution of relative width δ around ω_n. In these analyses the quadrupole moment value $Q = 0.83(13)b$ for the isomeric ^{111}Cd PAC state [18] was adopted, but its error was not taken into consideration. Further details of the equipment used and data analysis are presented in [6, 16].

3. Experimental results

3.1. Hafnium aluminides

Figure 3 illustrates PAC spectra, $R(t)$, and their Fourier transforms, $P(\omega)$, measured at 24 and 1073 K in the Hf_4Al_3 sample, which had been annealed for 1 day at 1373 K. The spectra are quite complex and exhibit four EFG fractions, one large fraction $f_1 = 60$–80% and three smaller fractions in the range of 5–20%. Their parameters are listed in table 1 and their assignments to lattice sites (in Hf_3Al_2) will be discussed in section 4. The evolutions of all four fractions f_i with the measuring temperature T_m are shown in figure 4; the fractions vary rather little with temperature.

In order to make the present results more transparent, we briefly refer to our previous analysis communicated in [11]. After 1 day of annealing the Hf_4Al_3 sample at 1223 K, the PAC spectrum taken at room temperature contained four EFG fractions, whose quadrupole parameters had been very similar to the ones previously found for ^{111}In/^{111}Cd probes in Hf_3Al_2 [9]. In the previously published analysis of the room-temperature data [11], the two largest fractions had been identified. Their quadrupole parameters were quoted as $\nu_{Q1} = 96.4(5)$ MHz and $\eta_1 = 0.69(1)$ for the largest fraction f_1 (possibly the Hf 4(g) site), and $\nu_{Q2} = 128(1)$ MHz and $\eta_2 = 0.44(1)$ for the second largest fraction f_2 (tentatively attributed to the Al 8(j) site). On the basis of these EFG

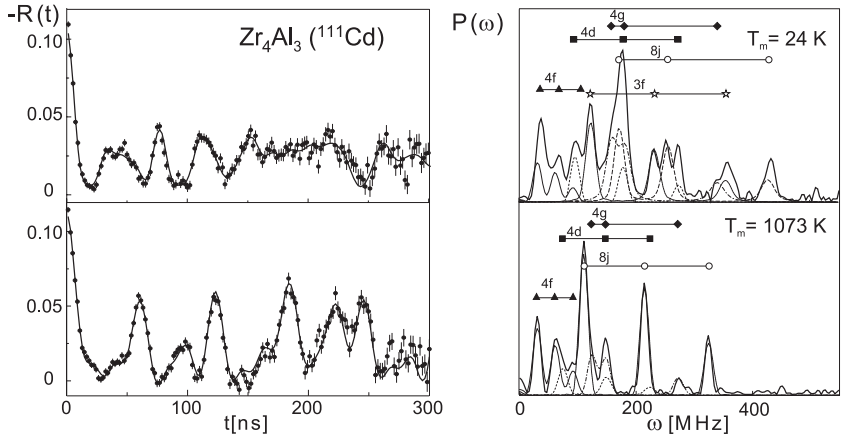

Figure 5. Same as figure 3 for the Zr_4Al_3 sample annealed at 1223 K.

Table 1. EFG parameters that characterize the hyperfine interactions (HFI) experimentally observed at ^{111}Cd probes in the mixed $(Hf/Zr)_4Al_3$–$(Hf/Zr)_3Al_2$ samples measured at room temperature and extrapolated to $T = 0$ K.

Sample	HFI	f (RT) (%)	ν_Q (RT) (MHz)	η (RT)	$\lvert V_{zz}\rvert$ (RT) (10^{21} V m^{-2})	$\lvert V_{zz}\rvert$ (0 K) (10^{21} V m^{-2})
Zr_4Al_3–Zr_3Al_2	1	21(3)	115(2)	0.21(5)	5.73(5)	5.9(1)
	2	15(5)	84(3)	0.08(5)	4.2(1)	4.5(2)
	3	23(2)	34(2)	0.30(3)	1.69(5)	1.7(1)
	4	15(2)	97.7(7)	0.92(4)	4.87(3)	5.1(1)
	5	26(3)	130(1)	0.30(4)	6.48(5)	6.9(1)
Hf_4Al_3–Hf_3Al_2	1	13(5)	88(5)	0	4.4(3)	4.3(4)
	2	7(2)	39(2)	0.12(5)	1.9(1)	2.0(2)
	3	63(3)	96.4(5)	0.69(3)	4.80(3)	5.0(1)
	4	20(2)	128(1)	0.44(2)	6.40(5)	6.7(1)

parameters, and especially the temperature evolution of the quadrupole frequencies, we had concluded that the ^{111}In impurities preferentially select sites in the minority phase Hf_3Al_2. On the other hand, it should be noted that—in agreement with the small Hf_3Al_2 phase admixture evidenced by XRD—the PAC spectra for ^{181}Hf $\rightarrow$ ^{181}Ta probes (self-atoms) in Hf_4Al_3 [2] had not shown any of the quadrupole frequencies characteristic of the Hf_3Al_2 phase [9].

3.2. Zirconium aluminides

Similar results had been reported for the mixed Zr_4Al_3 sample [11]. After the annealing at 1223 K, the room-temperature perturbation spectrum featured, besides several other components, quadrupole parameters similar to those measured in Zr_3Al_2. Further annealing for 3 days at 1293 K resulted in an increase of the fraction with $\nu_Q = 97.7(7)$ MHz and $\eta = 0.92(4)$ to about 50%, despite the decreasing Zr_3Al_2 phase admixture seen in the XRD spectrum (see figure 2).

The perturbation spectra and their Fourier transforms obtained at 24 and 1073 K measuring temperatures for this sample after the 1223 K annealing are presented in figure 5, while the temperature evolution of the fractions f_i (i = 1–5) is shown in figure 6. Again the assigned lattice sites will be discussed in section 4. Note that two of the fractions, labeled Al 8(j) and Al 3(f), vary quite strongly with the measuring temperature: the Al 3(f) fraction has disappeared around 600 K.

All the measured room-temperature EFG parameters are listed in table 1. Some of these parameters are slightly different from those communicated in the previous work [9, 11], due to the fact that in the new fits five instead of four EFG fractions were considered. The last column of table 1 lists the various EFGs extrapolated to $T = 0$, which are to be compared with the theoretical predictions for the various probe sites discussed below.

4. Theory

4.1. Procedure

The analysis of the PAC spectra for diffused ^{111}In $\rightarrow$ ^{111}Cd impurities in the mixed $(Hf/Zr)_4Al_3$ + $(Hf/Zr)_3Al_2$ samples after annealing at the higher temperatures gave evidence for up to five fractions, each with different EFG parameters. By comparison with the results of previous PAC studies on ^{111}In-doped single-phase $(Hf/Zr)_3Al_2$ samples [9], four of the fractions could each be assigned to the $(Hf/Zr)_3Al_2$ minority phases in the mixed samples. The most important aim of the theoretical work was to assign the measured EFGs to the possible crystallographic sites by performing *ab initio* electronic structure calculations in all the relevant compounds. To this end, we determined the self-consistent potentials and charge densities inside the Cd-doped $(Hf/Zr)_4Al_3$ and $(Hf/Zr)_3Al_2$ hosts and then calculated the EFG tensors at a Cd probe nucleus replacing either a single Hf/Zr or Al atom in the

Table 2. Calculated and experimentally determined structural parameters for $(Zr/Hf)_4Al_3$ and $(Zr/Hf)_3Al_2$. Experimental data were taken from [12].

		Theory	
	Experiment	LDA	CW-GGA
		Zr_4Al_3	
a	5.433 Å	5.418 Å	5.430 Å
c	5.390 Å	5.336 Å	5.394 Å
x	0.250	0.260	0.259
		Hf_4Al_3	
a	5.343 Å	5.262 Å	5.343 Å
c	5.422 Å	5.348 Å	5.476 Å
x	0.250	0.260	0.258
		Zr_3Al_2	
a	7.633 Å	7.661 Å	7.666 Å
c	6.996 Å	7.001 Å	6.980 Å
u	0.340	0.343	0.343
v	0.200	0.199	0.199
y	0.125	0.121	0.121
z	0.210	0.214	0.214
		Hf_3Al_2	
a	7.549 Å	7.571 Å	7.572 Å
c	6.909 Å	6.906 Å	6.905 Å
u	0.340	0.345	0.346
v	0.200	0.202	0.202
y	0.125	0.122	0.122
z	0.210	0.211	0.211

host lattice and taking properly into account the structural and electronic effects introduced by the impurity in the hosts. All the calculations refer to zero temperature and to substitutional probes.

As pointed out before the $(Hf/Zr)_4Al_3$ phase structure can be described as $P6/mmm$ (no. 191), with one 3f (mmm) Wyckoff position of low symmetry for Al and two axially symmetric positions for the Zr/Hf atoms, labeled 2d ($-6m2$) and 2e ($6mm$) [4, 11]. The 2e atoms are located at (0, 0, x), with $x = 1/4$. The 3f and 2d are located at (1/2, 0, 0) and (1/3, 2/3, 1/2), respectively. $(Hf/Zr)_3Al_2$ crystallizes in the tetragonal tP20-type structure (space group $P4_2/mnm$-D_{4h}^{14}), which possesses four non-equivalent crystallographic positions [4]: the Al atoms are in the 8(j) position of low symmetry, while the Hf/Zr atoms occupy either the axially symmetric 4(d) site or two sites of low $m2m$ symmetry labeled 4(f) and 4(g). The positions of all the atoms in the unit cell are determined by the four internal parameters u, v, y and z, namely Hf/Zr 4(f) (u, u, 0), Hf/Zr 4(g) (v, $1 - v$, 0) and Al 8(j) (y, y, z); the Hf/Zr 4(d) atoms are located at position (0, 1/2, 1/4). The experimental lattice parameters and the positional parameters u, v, y and z are listed in table 2.

In the case of $(Hf/Zr)_4Al_3$, the calculations were carried out considering a periodically repeated large supercell (SC), in which a Cd atom replaces a single host atom. Calculations were made for a periodic arrangement of 56-atom SCs, each constructed from eight unit cells of Hf_4Al_3 or Zr_4Al_3. The resulting SC has the dimensions $a' = 2a = 10.866$ Å, $b' = 2b = 10.866$ Å and $c' = 2c = 10.788$ Å (in the case of Zr_4Al_3) and $a' = 2a = 10.686$ Å, $b' = 2b = 10.686$ Å and $c' = 2c = 10.844$ Å (in the case of Hf_4Al_3) with a single host atom replaced by a Cd atom.

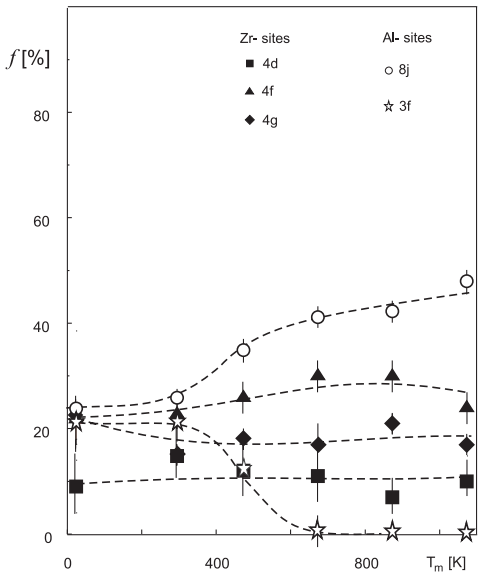

Figure 6. Temperature dependence of the ^{111}Cd probe fractions in the Zr_4Al_3 sample. The 4(d), 4(f), 4(g) and 8(j) crystallographic sites concern the Zr_3Al_2 minority phase admixture. The rapidly decreasing fraction we tentatively attribute to the Al 3(f) site in the Zr_4Al_3 majority phase.

For the $(Hf/Zr)_3Al_2$ phase, since here the unit cell dimensions are larger than those of the $(Hf/Zr)_4Al_3$ phase, the calculations were performed for two different Cd concentrations. In this way, we can study the effect of Cd concentration on the electronic and structural properties of these doped systems. Firstly, a Cd atom substitutes a single Hf/Zr or Al atom in the 20-atom unit cell, i.e. ordered $(Hf/Zr)_{11}CdAl_8$ or $(Hf/Zr)_{12}Al_7Cd$ alloys were considered. In a second approach, which approximates better $(Hf/Zr)_3Al_2$ with an *isolated* Cd impurity, we considered a periodically repeated larger supercell, in which a Cd atom replaces a single host atom. Calculations were made for a periodic arrangement of 160-atom supercells (SC), each constructed from eight unit cells of Hf_3Al_2 or Zr_3Al_2. The resulting SC has the dimensions $a' = 2a = 15.266$ Å, $b' = 2b = 15.266$ Å and $c' = 2c = 13.992$ Å (in the case of Zr_3Al_2) and $a' = 2a = 15.098$ Å, $b' = 2b = 15.098$ Å and $c' = 2c = 13.818$ Å (in the case of Hf_3Al_2) with a single host atom replaced by a Cd atom.

In all cases, although the Cd concentration is large compared with the parts-per-million (ppm) dilution in the samples used in the PAC experiments, the choice of the described SCs keeps the Cd atoms sufficiently far from each other (more than 10 Å) to avoid significant impurity–impurity interactions.

To solve the scalar-relativistic Kohn–Sham equations, calculations based on the density-functional theory (DFT) were performed with the augmented plane wave plus local orbital (APW + lo) method [14, 19] as embodied in the WIEN2K code [13]. In this method the wavefunctions are expanded in spherical harmonics inside non-overlapping atomic spheres

of radius R_{MT} and in plane waves in the remaining space of the unit cell (the interstitial region). Exchange and correlation effects were treated within the density-functional theory using the local density approximation (LDA) [20] and the recently proposed general gradient approximation of Wu and Cohen (WC-GGA) [21]. For all calculations presented in this paper, the atomic spherical radii used for Cd, Zr, Hf and Al were 1.3 Å. The parameter $Rk_{\max}$ which controls the size of the basis set, was fixed to 8.0 for the pure systems and the smallest cells. In the case of the 160-atom supercells, we used $Rk_{\max} = 7.0$ (R is the smallest muffin tin radius and $k_{\max}$ the largest wavenumber of the basis set). Integration in the reciprocal space was performed using the tetrahedron method taking up to 5000 k-points in the first Brillouin zone for the pure systems and the smallest cells and 200 k-points for the 160-atom SCs. Once self-consistency of the potential was achieved, quantum-mechanically derived forces were obtained and the ions were displaced according to a Newton-damped scheme, and then the new positions for the atoms were obtained; for details, see [22, 23]. The procedure was repeated until the forces on the ions were below a tolerance value fixed as 0.05 eV Å^{-1}; in the case of the pure systems, the tolerance value was reduced to 2 meV Å^{-1}. At each position the diagonal elements of the EFG tensor were obtained directly from the V_{2M} components of the lattice harmonic expansion of the self-consistent potential [24].

To check the accuracy of the results obtained in the 160-atom SCs, we performed several additional calculations. For selected cases, we varied the basis set (number of plane waves) from $Rk_{\max} = 5.0$ to 7.0. We also varied the number of k-points from 25 to 400. These variations showed that the EFGs and interatomic distances can be obtained with adequate precision using $Rk_{\max} = 6.0$ and 200 k-points; for those values the interatomic distances and the EFG components converged within about 0.01 Å and 0.5×10^{21} V m^{-2}, respectively. Structural relaxation, leading to forces on the atoms less than 0.05 eV Å^{-1}, is the most important factor for convergence of the electronic properties, and they do not produce significant changes by increasing the number of plane waves or of k-points.

4.2. Calculations for the undoped systems

In order to check the reliability of the theoretical approach, the equilibrium lattice parameters and positional parameters u, v, y and z in $(Hf/Zr)_3Al_2$ and x in $(Hf/Zr)_4Al_3$ were calculated. As the first step of this structural refinement, the atomic positions were relaxed. During this relaxation the lattice parameters and, as a consequence, the cell volume were kept fixed to their experimental values. Then the theoretical equilibrium volume was determined by fixing the atomic positions to their optimized values and further keeping the c/a ratio fixed. A series of calculations was carried out, in which the total energies were calculated as a function of the volume. In this way, we obtained the equilibrium volume (corresponding to the minimum energy). In the third step the c/a ratio was allowed to vary. Finally, the atomic positions were relaxed again, but now keeping the lattice parameters fixed at their optimized values. As can be seen in table 2, the lattice constants and the parameters u, v, y, z and x were found in excellent agreement with the experimental data. Additionally, the results obtained using LDA and CW-GGA turned out to be very similar. For these reasons and in order to make the various calculations in the doped systems comparable, we fixed in the following the lattice parameters at the experimental values.

Table 3. Optimized distances d^{rel} (in Å) of the Cd impurity to its four first shells of neighbors in Cd-doped $(Hf/Zr)_4Al_3$ compared with the ones in the pure systems (d^{pure}), calculated principal EFG component, V_{ZZ}, in units of 10^{21} V m^{-2}, and asymmetry parameter η at the Cd impurity. In brackets the type and multiplicity of neighbors. Results correspond to the 56-atom supercells.

Site	d^{pure}	d^{rel}	V_{ZZ}	η
		Zr_4Al_3		
Al 3f	2.66 Å [Al, 4]	2.72 Å [Al, 4]	+5.32	0.82
	3.00 Å [Zr, 4]	3.06 Å [Zr, 4]		
	3.08 Å [Zr, 4]	3.12 Å [Zr, 4]		
	4.61 Å [Al, 4]	4.71 Å [Al, 4]		
	4.76 Å [Zr, 4]	4.82 Å [Zr, 4]		
Zr 2d	3.07 Å [Zr, 3]	3.15 Å [Al, 6]	+8.6	0
	3.08 Å [Al, 6]	3.18 Å [Zr, 3]		
	3.33 Å [Zr, 6]	3.39 Å [Zr, 6]		
	4.86 Å [Al, 12]	4.86 Å [Al, 12]		
Zr 2e	2.55 Å [Zr, 1]	2.68 Å [Zr, 1]	−0.03	0
	2.77 Å [Zr, 1]	2.81 Å [Zr, 1]		
	3.00 Å [Al, 6]	3.12 Å [Al, 6]		
	3.30 Å [Zr, 6]	3.36 Å [Zr, 6]		
	4.76 Å [Al, 6]	4.95 Å [Al, 6]		
		Hf_4Al_3		
Al 3f	2.63 Å [Al, 4]	2.68 Å [Al, 4]	+5.63	0.91
	2.97 Å [Hf, 4]	3.03 Å [Hf, 4]		
	3.08 Å [Hf, 4]	3.14 Å [Hf, 4]		
	4.56 Å [Al, 4]	4.63 Å [Al, 4]		
Hf 2d	3.04 Å [Hf, 3]	3.10 Å [Hf, 3]	+8.8	0
	3.07 Å [Al, 6]	3.18 Å [Al, 6]		
	3.30 Å [Hf, 6]	3.36 Å [Hf, 6]		
	4.83 Å [Al, 12]	4.90 Å [Al, 12]		
Hf 2e	2.57 Å [Hf, 1]	2.67 Å [Hf, 1]	−2.5	0
	2.77 Å [Hf, 1]	2.82 Å [Hf, 1]		
	2.97 Å [Al, 6]	3.08 Å [Al, 6]		
	3.30 Å [Hf, 6]	3.34 Å [Hf, 6]		

4.3. Calculations in the doped systems

After the study of the pure systems, we substituted an Hf/Zr or Al host atom by a Cd probe atom in the unit cells of $(Hf/Zr)_4Al_3$ and $(Hf/Zr)_3Al_2$, as described before. This substitution produces non-negligible forces on its nearest neighbors. We have to remark that even small changes in the atomic positions can induce large effects on the EFG and even more on the asymmetry parameter. For these reasons, full relaxation of all atomic positions were considered, until forces on the atoms were below 0.05 eV Å^{-1}. We use this tolerance criterion because a displacement induced by forces smaller than this limit produces changes in the EFG components that are below the convergence error. As in the case of the pure

Table 4. Same as table 3 for the pure and Cd-doped $(Hf/Zr)_3Al_2$ systems. The results were obtained at the relaxed structures of the 20-atom supercells. In brackets the type and multiplicity of neighbors.

		LDA			CW-GGA		
Site	d^{pure}	d^{rel}	V_{ZZ}	η	d^{rel}	V_{ZZ}	η
			Zr_3Al_2				
Al 8(j)	2.61 [Al]	2.66 [Al]	+5.1	0.08	2.65 [Al]	+5.1	0.09
	2.78 [Zr]	2.84 [Zr]			2.84 [Zr]		
	2.83 [Zr]	2.87 [Zr]			2.88 [Zr]		
	2.93 [Zr, 2]	2.95 [Zr, 2]			2.95 [Zr, 2]		
Zr 4(d)	3.05 [Al, 4]	3.11 [Al, 4]	−4.4	0	3.10 [Al, 4]	−4.3	0
	3.26 [Zr, 4]	3.24 [Zr, 4]			3.25 [Zr, 4]		
	3.37 [Zr, 4]	3.38 [Zr, 4]			3.38 [Zr, 4]		
	3.50 [Zr, 2]	3.50 [Zr, 2]			3.50 [Zr, 2]		
Zr 4(f)	2.83 [Al, 2]	2.86 [Al, 2]	+2.2	0.76	2.86 [Al, 2]	+2.2	0.74
	2.93 [Al, 4]	2.90 [Al, 4]			2.90 [Al, 4]		
	3.37 [Zr, 4]	3.34 [Zr]			3.35 [Zr]		
	3.38 [Zr]	3.38 [Zr, 4]			3.38 [Zr, 4]		
Zr 4(g)	2.78 [Al, 2]	2.70 [Al, 2]	−4.0	0.80	2.71 [Al, 2]	−3.9	0.80
	2.93 [Al, 4]	3.01 [Al, 4]			3.00 [Al, 4]		
	3.26 [Zr, 4]	3.24 [Zr, 4]			3.24 [Zr, 4]		
	3.53 [Zr, 2]	3.55 [Zr, 2]			3.54 [Zr, 2]		
			Hf_3Al_2				
Al 8(j)	2.60 [Al]	2.63 [Al]	+3.9	0.08	2.61 [Al]	+3.8	0.11
	2.75 [Hf]	2.76 [Hf]			2.75 [Hf]		
	2.80 [Hf]	2.83 [Hf]			2.82 [Hf]		
	2.90 [Hf, 2]	2.96 [Hf, 2]			2.95 [Hf, 2]		
Hf 4(d)	3.01 [Al, 4]	3.06 [Al, 4]	−4.2	0	3.06 [Al, 4]	−4.2	0
	3.22 [Hf, 4]	3.22 [Hf, 4]			3.21 [Hf, 4]		
	3.34 [Hf, 4]	3.39 [Hf, 4]			3.40 [Hf, 4]		
	3.45 [Hf, 4]	3.45 [Hf, 4]			3.45 [Hf, 4]		
Hf 4(f)	2.80 [Al, 2]	2.83 [Al, 2]	+1.2	0.37	2.82 [Al, 2]	+1.3	0.44
	2.90 [Al, 4]	2.85 [Al, 4]			2.85 [Al, 4]		
	3.31 [Hf]	3.29 [Hf]			3.28 [Hf]		
	3.34 [Hf, 4]	3.38 [Hf, 4]			3.38 [Hf, 4]		
Hf 4(g)	2.74 [Al, 2]	2.66 [Al, 2]	+3.8	0.97	2.67 [Al, 2]	+3.8	0.91
	2.91 [Al, 4]	2.98 [Al, 4]			2.98 [Al, 4]		
	3.22 [Hf, 4]	3.23 [Hf, 4]			3.21 [Hf, 4]		
	3.49 [Hf, 2]	3.52 [Hf, 2]			3.52 [Hf, 2]		

systems, both the LDA and CW-GGA were applied. Only small differences in V_{ZZ} of the order of 0.1×10^{21} V m^{-2} and in the optimized distances (d^{rel}) by up to 0.01 Å were found between LDA and CW-GGA, while the asymmetry parameters were quite stable, providing differences between LDA and CW-GGA smaller than 0.02. Since the two approaches for the exchange and correlation potential gave differences of the order of the convergence errors, for simplicity only those obtained with LDA will be discussed here.

In order to find out which of the measured hyperfine interactions correspond to the majority phases $(Hf/Zr)_4Al_3$, and which to the minority phases $(Hf/Zr)_3Al_2$, the EFGs of Cd located at all possible crystallographic sites in all phases were calculated. We first present the results in the $(Hf/Zr)_4Al_3$ majority phases by showing in table 3 the relaxations of the Cd nearest neighbors (four shells of neighbors). In both Zr_4Al_3 and Hf_4Al_3 the structural distortions are quite anisotropic. As an example, in the case of the Zr 2d site the equilibrium Cd–Zr distance gets larger than the Cd–Al distance, in contrast to the unrelaxed structure.

The calculated EFG values for Cd at the three sites of $(Hf/Zr)_4Al_3$ are also listed in table 3. We first note that the calculations do not reproduce the measured EFGs (compare the experimental results of table 1 and APW + lo predictions in table 3). Regarding the typical accuracy of a few per cent for the calculated EFGs, no reliable site assignment is possible here. Only the EFG fraction observed in Zr_4Al_3 and characterized by $\nu_Q = 115$ MHz and $\eta = 0.21$ (HFI *bI*) may be tentatively assigned to the Al 3f site, although the predicted asymmetry parameter deviates from the experimental value.

In view of these negative results, we extended the calculations to the minority phases, $(Hf/Zr)_3Al_2$, by considering the two different Cd concentrations discussed before. The results obtained for the structural distortions as well as the values of V_{ZZ} and η for the 20-atom cells are reported in table 4. The Cd concentration in this case is far too high to allow a meaningful comparison with the PAC experiments for dilute systems. For this cell size, the interaction between Cd neighbors cannot be neglected and the structural relaxation of the Cd nearest-neighbor atoms is constrained by the large Cd concentration

Table 5. Optimized distances d (in Å) of the Cd impurity to its four first shells of neighbors in Cd-doped $(Hf/Zr)_3Al_2$, calculated principal EFG component, V_{ZZ}, in units of 10^{21} V m^{-2}, and asymmetry parameter η at the Cd impurity. The theoretical results are compared with the experimental PAC results (extrapolated to 0 K). The results correspond to the relaxed structures of the 160-atom supercells.

		Theory			Experiment (0 K)	
System	Site	d	V_{ZZ}	η	V_{ZZ}	η
Zr_3Al_2	Al 8(j)	2.64 [Al] 2.85 [Zr] 2.85 [Zr] 2.89 [Zr, 2]	+6.9	0.26	6.9(1)	0.30(4)
	Zr 4(d)	3.07 [Al, 4] 3.27 [Zr, 4] 3.40 [Zr, 4] 3.55 [Zr, 2]	−3.7	0.00	4.5(2)	0.08(5)
	Zr 4(f)	2.84 [Al, 2] 2.94 [Al, 4] 3.27 [Zr] 3.37 [Zr, 4]	+1.5	0.34	1.7(1)	0.30(3)
	Zr 4(g)	2.69 [Al, 2] 2.96 [Al, 4] 3.25 [Zr, 4] 3.56 [Zr, 2]	−4.6	0.85	5.1(1)	0.92(4)
Hf_3Al_2	Al 8(j)	2.62 [Al] 2.79 [Hf] 2.80 [Hf] 2.89 [Hf, 2]	+6.7	0.10	6.7(1)	0.44(2)
	Hf 4(d)	3.03 [Al, 4] 3.24 [Hf, 4] 3.36 [Hf, 4] 3.50 [Hf, 2]	−3.9	0.00	4.3(2)	0.00
	Hf 4(f)	2.81 [Al, 2] 2.90 [Al, 4] 3.24 [Hf] 3.41 [Hf, 4]	+1.1	0.17	2.0(1)	0.12(5)
	Hf 4(g)	2.66 [Al, 2] 2.95 [Al, 4] 3.25 [Hf, 4] 3.54 [Hf, 2]	+4.6	0.62	5.0(1)	0.69(3)

and the spurious interaction between relaxing atoms. Therefore calculations using the much larger SC were performed. Comparing the equilibrium Cd-bond lengths for the two cell sizes, it is seen in tables 4 and 5 that there are small differences, which exceed the convergence errors. In conclusion and not unexpectedly the structural distortion induced by the Cd probe depends on the impurity concentration. As the EFG generally decays as r^{-3}, where r is the distance from the producing charge density, it is particularly sensitive to slight local changes, especially in the first shells of neighbors. For this reason, the structural distortions must be carefully calculated when comparing the EFG predictions with the experimental results.

In table 5, the calculated EFG tensors at the Cd sites in the equilibrium structures of $(Hf/Zr)_3Al_2$ using the 160-atom SCs are summarized, which again illustrate the strong dependence on the Cd concentration. Since different concentrations produce different structural distortions, it is interesting to separate the electronic and structural effects. As a test case, we considered the 20-atom cell of Zr_3Al_2, but fixed the Cd atom and its nearest neighbors at the equilibrium positions predicted for the 160-atom SC and calculated the EFG tensors for this geometry at all four possible Cd sites. As a result, for identical geometries of Cd, significant differences in the EFGs occur between the 20-atom and 160-atom SC. This calculation proves the relevance of the large Cd–Cd interaction in the case of the smaller cell, which affects the EFG even when identical ion positions are used, besides the effects of structural distortions based on different impurity concentration. Similar conclusions were drawn in the case of Hf_3Al_2.

Finally, by comparing the measured EFG parameters with the ones obtained from APW + lo we can now assign the observed hyperfine interaction fractions to the various crystallographic sites in $(Hf/Zr)_3Al_2$. As illustrated in table 5, the theoretical predictions are in most cases in very good agreement with the experiments. However, deviations were found for the site Zr 4(d) in Zr_3Al_2 and the sites Al 8(j) and Hf 4(f) in Hf_3Al_2. In the first case, the discrepancy in V_{ZZ} amounts to about 20%, while in the last case, we find a serious discrepancy by a factor of two, probably due to the small value of V_{ZZ} at this site. For the purpose of this paper, we judge the few deviations as acceptable considering the complex mixed phases treated.

Table 6. Calculated substitution energies of an In atom at the various sites in the $(Hf/Zr)_4Al_3$ and $(Hf/Zr)_3Al_2$. Results are obtained with the LDA approach and relaxed 160-atom supercell.

Phase	Site	Substitution energy (eV)
Hf_4Al_3	Hf 2(d)	1.8
	Hf 2(e)	1.7
	Al 3(f)	2.7
Hf_3Al_2	Hf 4(d)	2.2
	Hf 4(f)	2.3
	Hf 4(g)	1.1
	Al 8(j)	2.7
Zr_4Al_3	Zr 2(d)	5.8
	Zr 2(e)	5.9
	Al 3(f)	2.5
Zr_3Al_2	Zr 4(d)	4.8
	Zr 4(f)	5.2
	Zr 4(g)	5.6
	Al 8(j)	2.7

4.4. Phase preference of In dopants

If the various lattice sites in the mixed compounds were randomly occupied by the $^{111}In(\rightarrow{}^{111}Cd)$ probes, the sites corresponding to the $(Hf/Zr)_4Al_3$ majority phases should be much more strongly populated. This is opposite to the experimental finding of the PAC measurements that the ^{111}In impurities, after the high temperature annealing, end up nearly exclusively on the sites in the $(Hf/Zr)_3Al_2$ minority phases. Note that, in order to explain this preferential site occupation, we have to consider the radioactive father of ^{111}Cd, namely ^{111}In, thus making the reasonable assumption that the $^{111}In \rightarrow {}^{111}Cd$ electron capture decay does not change the lattice sites selected by indium.

Table 7. *Ab initio* based final assignments of the hyperfine interactions (HFI) experimentally observed at ^{111}Cd probes in the mixed $(Hf/Zr)_4Al_3$–$(Hf/Zr)_3Al_2$ samples to crystallographic sites.

Sample	HFI	f (RT) (%)	ν_Q (RT) (MHz)	η (RT)	$\lvert V_{zz}\rvert$ (RT) (10^{21} V m^{-2})	Site
Zr_4Al_3–Zr_3Al_2	1	21(3)	115(2)	0.21(5)	5.73(5)	Al 3f
	2	15(5)	84(3)	0.08(5)	4.2(1)	Zr 4(d)
	3	23(2)	34(2)	0.30(3)	1.69(5)	Zr 4(f)
	4	15(2)	97.7(7)	0.92(4)	4.87(3)	Zr 4(g)
	5	26(3)	130(1)	0.30(4)	6.48(5)	Al 8(j)
Hf_4Al_3–Hf_3Al_2	1	13(5)	88(5)	0.00	4.4(3)	Hf 4(d)
	2	7(2)	39(2)	0.12(5)	1.9(1)	Hf 4(f)
	3	63(3)	96.4(5)	0.69(3)	4.80(3)	Hf 4(g)
	4	20(2)	128(1)	0.44(2)	6.40(5)	Al 8(j)

In order to understand the site selection, we performed *ab initio* total energy calculations for In-doped $(Hf/Zr)_4Al_3$ and $(Hf/Zr)_3Al_2$ compounds, in which In occupies the seven possible lattice locations in each mixed sample. The calculations were performed using the 56-atom SC in $(Hf/Zr)_3Al_2$ and the 160-atom Sc in $(Hf/Zr)_4Al_3$, with the same precision as that corresponding to the Cd impurities. The structural distortions induced by the In impurities in the host were also computed.

In order to estimate the preferred site occupation, we compared the defect formation energies, i.e. the substitution energies, E_{subst}, for both phases using the expression

$$E_{subst} = E^{tot}_{subst} - E_{In} + E_X - E_{pure}. \quad (2)$$

Here E^{tot}_{subst} is the total energy of the supercell containing a single substitutional In atom, E_{In} and E_X denote the energies of an In impurity and Hf/Zr or Al atom, and E_{pure} is the energy of the considered supercell without impurities. The substitution energies were obtained by calculating the energies of undoped $(Hf/Zr)_4Al_3$ and $(Hf/Zr)_3Al_2$ compounds, E_{pure}, and E_{In} and E_X from metallic In, Hf, Zr and Al with the same precision as that in the supercells. The convergence errors in the substitution energies are around 0.3 eV. In passing we note that small values of the substitution energies indicate preferential replacement of a host atom by indium, although the approach does not allow us to quantitatively estimate the hyperfine fractions.

The obtained defect formation energies for each site in all the compounds are reported in table 6. In the mixed Hf_4Al_3–Hf_3Al_2 sample, the substitution energy for the Hf 4(g) site in Hf_3Al_2 is the smallest one. Based on this argument, we may explain the preferential site occupation of this site observed in the PAC experiments (see table 1). In the case of Zr_4Al_3–Zr_3Al_2, the smallest substitution energies correspond to the Al 3(f) site in Zr_4Al_3 and the Al 8(j) site in Zr_3Al_2. Again, when comparing the measured hyperfine interaction fractions with the ones expected on the basis of the total energy calculations, we can see that the interactions associated with Cd in the Al sites are those with larger populations, in agreement with our calculations for the substitution energies. The other interactions associated with the Zr 4(d), Zr 4(f) and Zr 4(g) have similar populations. Comparing to the calculated substitution energies, we see that the substitution energies for these sites are smaller than those for Cd substitutionally located in the Zr sites (Zr 2(d) and Zr 2(e)) of the Zr_4Al_3 phase.

In conclusion, the calculations of substitution energies make plausible the observed preference of In probes for the crystallographic sites in $(Hf/Zr)_3Al_2$. In light of the theoretical calculations performed here, the assignments of the hyperfine interactions observed in the PAC experiments can be done and are summarized in table 7.

5. Summary and conclusions

Hyperfine interactions and, in particular, electric field gradients constitute a very sensitive tool to investigate the local environment of probe nuclei; their measurement can provide detailed information on structural and electronic properties of the system under study. In a well-defined single-phase crystal with known lattice structure the interpretation of such measurements is usually not too difficult, but even here situations may occur, where distinguishable hyperfine fractions must be assigned to different lattice sites. In more complicated cases with impurities, point defects, multi-phase samples or systems with more than one crystallographic site, the interpretation of the various EFG fractions is by no means straightforward. Arguments based on point charge summations or symmetry considerations may fail, since the chemical nature of the impurity is not taken into account which, through structural distortions of its neighborhood, may strongly affect the EFG. To unravel these complex cases, a realistic theory is of great help, which models different structural and electronic scenarios.

The present work concerns such complex systems, namely coexistent Hf–Al intermetallic phases: samples of $(Hf/Zr)_4Al_3$ containing small amounts of $(Hf/Zr)_3Al_2$ and doped with low concentrations of the PAC probes $^{111}In \rightarrow {}^{111}Cd$. In principle, the impurity probe atoms can populate seven different crystallographic sites in these compounds. PAC revealed up to five EFG components in each sample. To assign these hyperfine interactions to the crystallographic sites, DFT calculations of electronic structure and atomic forces have been used to describe $(Hf/Zr)_4Al_3$ and $(Hf/Zr)_3Al_2$ in their pure forms as well as with substitutional Cd and In impurities.

In this work, only substitutional In and Cd probe impurities were considered, replacing an Hf/Zr or Al atom, and the supercell approach was employed. Although in theory

the impurity concentration is considerably larger than in the experiment, the 56-atom and 160-atom supercell calculations used in the case of $(Hf/Zr)_4Al_3$ and $(Hf/Zr)_3Al_2$ yield results that sufficiently converged to allow comparison to the data. For all the systems, the defect structures were optimized using force calculations and from the self-consistent potentials the EFG were derived, allowing us a direct comparison to the experimental EFGs.

In the case of the pure systems, APW + lo correctly predicts the lattice parameters and internal positions of the Hf, Zr and Al atoms. Additionally, LDA and CW-GGA predict very similar equilibrium structures. Concerning the doped systems, the Cd impurities were found to induce sizable structural distortions in the host lattices. The relaxed distances were found almost independent of the approximations employed for the correlation and exchange potential. Due to the r^{-3} dependence of the EFG operator, the EFG is very sensitive to fine details of the atomic positions. Finally, we found that the calculations performed here (LDA, WC-GGA) predict almost the same EFGs for the equilibrium structures of Cd-doped Zr_4Al_3. This statement is also valid in the case of Hf_4Al_3 and the 3–2 phases (Cd-doped Zr_3Al_2 and Hf_3Al_2). Again, due to the fact that the EFG is very sensitive to small changes in the electronic charge density, we may conclude that these calculations give very similar descriptions of the electronic structures of each system.

The calculated substitution energies suggest that In prefers to locate at the Hf 4(g) sites in the Hf_3Al_2–Hf_4Al_3 sample. For this site, the substitution energy is 1.1 eV, which is at least 0.6 eV (which corresponds to at least 30%) smaller than the other ones. This fact explains the site preference of the $^{111}In \rightarrow {}^{111}Cd$ probes (63% of the population observed in the experiments). The case of the Zr_3Al_2–Zr_4Al_3 sample is more subtle: the calculated substitution energies suggest that In prefers either the Al 8(j) or Al 3(f) sites, but these energies are very close together. In addition, the calculations for the Cd-doped compounds allowed us to assign a total of at least eight hyperfine interactions to the various inequivalent sites of these phases. These detailed calculations for solute In atoms in the $(Hf/Zr)_3Al_2$ and $(Hf/Zr)_4Al_3$ intermetallics, compared with TDPAC measurements, indicate that the In mother probes predominantly populate the sites in the minority phases $(Hf/Zr)_3Al_2$.

Acknowledgments

This work was partially supported by Agencia Nacional de Promoción Científica y Tecnológica (ANPCyT) (PICT98 03-03727), Consejo Nacional de Investigaciones Científicas y Técnicas (CONICET)(PIP6032 and 0002), Fund. Antorchas, Argentina, and Third World Academy of Sciences (TWAS), Italy (RGA 97-057), Cnpq, Fapesp and Capes (Brazil). This research made use of the HP-Parallel-Computing Bose Cluster and the computational facilities of the Physics of Impurities (PhI group) at IFLP and Departamento de Física (UNLP) and at LCCA-USP. We acknowledge support by Deutsche Forschungsgemeinschaft (DFG) and Deutscher Akademischer Austauschdienst (DAAD). JB-C and VK acknowledge the support from the Serbian Ministry of Science.

References

[1] Collins G and Zacate M 2001 *Hyperfine Interact.* **136/137** 641
Collins G and Zacate M 2001 *Hyperfine Interact.* **136/137** 647
[2] Wodniecki P, Kulińska S, Wodniecka B, Cottenier S, Petrilli H M, Uhrmacher M and Lieb K P 2007 *Europhys. Lett.* **77** 43001
[3] Kulińska A, Wodniecki P, Wodniecka B, Petrilli H M, Terrazos L A, Uhrmacher M and Lieb K P 2009 *J. Phys.: Condens. Matter* **21** 506001
[4] Villars P and Calvert L D 1991 *Pearson's Handbook of Crystallographic Data for Intermetallic Phases* (Materials Park, OH: ASM)
Okamoto H 2000 *Phase Diagrams for Binary Alloys* (Materials Park, OH: ASM)
[5] Wodniecki P, Wodniecka B, Kulińska A, Uhrmacher M and Lieb K P 2000 *J. Alloys Compounds* **312** 17
Wodniecki P, Wodniecka B, Kulińska A, Uhrmacher M and Lieb K P 2001 *Hyperfine Interact.* **136/137** 535
[6] Wodniecki P, Wodniecka B, Kulińska A, Uhrmacher M and Lieb K P 2001 *Phys. Lett.* A **288** 227
Wodniecki P, Wodniecka B, Kulińska A, Uhrmacher M and Lieb K P 2002 *J. Alloys Compounds* **335** 20
[7] Wodniecki P, Wodniecka B, Kulińska A, Uhrmacher M and Lieb K P 2003 *J. Alloys Compounds* **351** 1
[8] Wodniecki P, Wodniecka B, Kulińska A, Uhrmacher M and Lieb K P 2004 *J. Alloys Compounds* **365** 52
[9] Wodniecki P, Kulińska A, Wodniecka B, Uhrmacher M and Lieb K P 2005 *Hyperfine Interact.* **158** 429
Wodniecki P, Kulińska A, Wodniecka B, Uhrmacher M and Lieb K P 2005 *Hyperfine Interact.* **158** 339
[10] Belosevic-Cavor J, Koteski V, Cekic B and Umecevic A 2007 *Comput. Mater. Sci.* **41** 164
[11] Wodniecki P, Kulińska A, Wodniecka B, Uhrmacher M and Lieb K P 2007 *Hyperfine Interact.* **177** 111
[12] Cenzual K, Gelato L M, Penzo M and Parthe E 1991 *Acta Crystallogr.* B **47** 433
[13] Blaha P, Schwarz K, Madsen G, Kvasnicka D and Luitz J 2001 *WIEN2k, an Aug-Plane Wave + Local Orbitals Program for Calculating Crystal Properties* Technische Universität Wien (ISBN 3-9501031-1-2)
[14] Madsen G K H, Blaha P, Schwarz K, Sjöstedt E and Nordström L 2001 *Phys. Rev.* B **64** 195134
[15] Slater J C 1964 *J. Chem. Phys.* **39** 3199
[16] Frauenfelder H and Steffen R 1963 *Alfa-, Beta- and Gamma-Ray Spectroscopy* vol 2, ed K Siegbahn (Amsterdam: North-Holland) p 917
[17] Mendoza-Zélis L A, Bibiloni A G, Caracoche M C, López-García A R, Martínez J A, Mercader R C and Pasquevich A F 1977 *Hyperfine Interact.* **3** 315
[18] Herzog P, Freitag K, Reuschenbach M and Walitzki H 1980 *Z. Phys.* A **294** 13
[19] Andersen O K 1975 *Phys. Rev.* B **12** 3060
Sjöstedt E, Nordström L and Singh D J 2000 *Solid State Commun.* **114** 15
See also Cottenier S 2002 *Density Functional Theory and the Family of (L)APW-Methods: A Step-by-Step Introduction* KU Leuven, Belgium http://www.wien2k.at/reg_user/textbooks
[20] Perdew J P and Wang Y 1992 *Phys. Rev.* B **45** 13244
[21] Wu Z and Cohen R E 2006 *Phys. Rev.* B **73** 235116
[22] Errico L A, Fabricius G, Rentería M, de la Presa P and Forker M 2002 *Phys. Rev. Lett.* **89** 055503
Errico L A, Fabricius G and Rentería M 2003 *Phys. Rev.* B **67** 144104
[23] Terrazos L A, Petrilli H M, Marszalek M, Saitovich H, Silva P R J, Blaha P and Schwarz K 2002 *Solid. State Commun.* **121** 525
[24] Schwarz K, Ambrosch-Draxl C and Blaha P 1992 *Phys. Rev.* B **42** 2051
Schwarz K, Ambrosch-Draxl C and Blaha P 1992 *Phys. Rev.* B **46** 1321